Am J Cancer Res 2026;16(4):1567-1588
www.ajcr.us /ISSN:2156-6976/ajcr0171634

Original Article

Coptisine suppresses oral squamous cell carcinoma via regulating the JAK2/STAT3 to induce mitochondrial dysfunction in cancer cells and promote macrophage polarization to M1

Feng Liu, Wei Wang, Wanwan Tian

Department of Acupuncture and Massage, Henan Vocational College of Tuina, No. 10, Xuefu Street, Luolong District, Luoyang 471023, Henan, China

Received January 22, 2026; Accepted April 14, 2026; Epub April 25, 2026; Published April 30, 2026

Abstract: Coptisine (COP) is an isoquinoline alkaloid with anti-tumor potential. However, its function and specific mechanisms in oral squamous cell carcinoma (OSCC), particularly its role in regulating the tumor microenvironment, remain unclear. The optimal intervention dose of COP was determined using the Cell Counting Kit-8 (CCK-8) assay. The effects of COP on the malignant phenotype of OSCC cells were evaluated by wound healing assay, flow cytometry, and Transwell assays. Mitochondrial function was evaluated using Seahorse energy metabolic analysis, commercial assay kits, and reactive oxygen species (ROS) detection. A co-culture system of THP-1-derived macrophages and OSCC cells was established, and the polarization phenotype was analyzed using flow cytometry and Western blotting. The mitochondrial-targeted antioxidant MitoQ, the pathway inhibitor AG490, and the activator Colivelin were used in rescue experiments to demonstrate the key roles of the Janus kinase 2/signal transducer and activator of transcription 3 (JAK2/STAT3) axis. COP at concentrations of 25, 50 and 100 μM significantly suppressed proliferation and epithelial-mesenchymal transition (EMT) and promoted apoptosis in OSCC cells. Mechanistically, COP inhibited JAK2/STAT3 signaling, reduced adenosine triphosphate (ATP) production and mitochondrial membrane potential (MMP), and increased ROS levels, thereby inducing mitochondrial dysfunction and ultimately inhibiting the growth of SCC-9 cells; MitoQ reversed these effects. Within the tumor microenvironment, COP also inhibited the JAK2/STAT3 pathway in macrophages, promoted its polarization toward M1 type, and inhibited its conversion to M2 type. Co-culture with M1 macrophages significantly attenuated the malignant phenotype of SCC-9 cells, which was reversed by Colivelin. In summary, COP exerts dual anti-OSCC effects by inducing mitochondrial dysfunction and oxidative stress through inhibition of the JAK2/STAT3 signaling pathway, as well as by promoting the polarization of macrophages toward the M1 anti-tumor phenotype via the same pathway.

Keywords: Coptisine, oral squamous cell carcinoma, mitochondria, macrophages, Janus kinase 2/signal transducer and activator of transcription 3 signaling pathway

Introduction

Oral squamous cell carcinoma (OSCC) is a malignant tumor derived from squamous epithelium of the lip, buccal mucosa, tongue, palate, and maxillofacial skin [1, 2]. The global annual incidence of oral cancer is approximately 389,000, ranking 16th among all malignancies, with a death toll of 188,000, ranking 14th in cancer-related mortality [3]. Despite rapid advances in therapeutic strategies and techniques, the mortality rate of OSCC remains high, primarily due to its aggressive invasiveness, early propensity for lymph node metastasis, and resistance to traditional chemotherapeutic agents. Consequently, patients often exhibit unfavorable prognosis, and postoperative quality of life remains unsatisfactory [4, 5]. Therefore, the treatment and prognosis of OSCC continue to face severe challenges.

Normal mitochondrial function is essential for cellular processes, including metabolism, proliferation, migration, and apoptosis. Disruption of these processes can lead to mitochondrial dysfunction, thereby contributing to tumorigenesis.

https://doi.org/10.62347/YYTC4227

Oxidative stress represents a key cellular response to pathological stimulation and is manifested by excessive production of reactive oxygen species (ROS), which promotes the formation of a tumor-supportive microenvironment [6]. ROS accumulation induces mitochondrial DNA damage, leading to progressive dysfunction of the respiratory chain, alterations in mitochondrial dynamics, and abnormalities in mitochondrial membrane potential (MMP). In turn, mitochondrial dysfunction aggravates oxidative stress and contributes to the progression of OSCC [7, 8]. Therefore, targeting mitochondrial dysfunction may represent a potential strategy to inhibit OSCC development.

Tumor development depends not only on the intrinsic proliferative capacity of cancer cells but also on interactions within the tumor microenvironment (TME). Tumor-associated macrophages (TAMs), which infiltrate tumor tissues, play critical roles in regulating tumor immune responses and are strongly associated with OSCC invasion and metastasis. TAMs are generally divided into two phenotypes due to their heterogeneity, namely M1 type and M2 type. M1 macrophages exert anti-tumor effects by promoting inflammatory response, whereas M2 macrophages facilitate tumor growth and metastasis by suppressing inflammatory response [9-11]. M1 macrophages can produce a variety of pro-inflammatory cytokines, including inducible nitric oxide synthase (iNOS), interleukin-6 (IL-6), and tumor necrosis factor-α (TNF-α) [12, 13]. Studies have demonstrated that promoting TAM polarization to M1 phenotype can inhibit the invasion and metastasis of OSCC [14], which may represent a promising therapeutic strategy for OSCC.

The Janus kinase 2 (JAK2)/signal transducer and activator of transcription 3 (STAT3) axis is a critical intracellular signaling pathway involved in the regulation of tumorigenesis and development through modulation of multiple downstream effectors [15, 16]. Persistent activation of JAK2/STAT3 signaling has been observed in OSCC and contributes to tumor progression and metastasis [17]. Previous studies have reported that inhibiting JAK2/STAT3 signaling can suppress macrophage M2 polarization and malignant phenotypes, including tumor cell proliferation and invasion [18]. In addition, this signaling is closely associated with mitochondrial function. Inhibition of this pathway has been reported to alleviate mitochondrial dysfunction and regulate necroptosis [19]. Targeting this axis, along with activation of mitochondrial apoptosis, has been proposed as a therapeutic strategy for hepatocellular carcinoma [20].

Natural products have garnered significant attention in tumor therapy due to their multi-target properties and relatively low toxicity. Coptisine (COP) is an isoquinoline alkaloid extracted from traditional Chinese medicines such as *Coptis chinensis and Phellodendron amurense*, and exhibits extensive biological activities. COP has been reported to exert anti-inflammatory, anti-oxidant, hypoglycemic, and anti-tumor effects [21]. In terms of its anti-tumor effects, COP has been shown to inhibit the growth of various malignant tumor cells through mechanisms including cell cycle arrest, suppression of angiogenesis, and inhibition of tumor cell metastasis [22-24]. Notably, COP can also induce mitochondrial dysfunction and ROS production in tumor cells [25]. Given its favorable safety profile and low toxicity, COP represents a promising candidate for novel anti-tumor drug development.

However, the inhibitory effects of COP on OSCC and the underlying mechanisms remain incompletely elucidated. Therefore, in this study, human OSCC cells and human mononuclear leukemia cells (THP-1) were utilized to establish *in vitro* models. We aimed to investigate the effects of COP on malignant phenotypes, mitochondrial dysfunction, macrophage polarization, and the JAK2/STAT3 signaling pathway in OSCC. This study seeks to offer experimental bases for the application of COP in OSCC therapy.

Methods

Cell model and grouping

Human monocytic leukemia THP-1 and OSCC cell lines (SCC-25 and SCC-4) were obtained from SUNNCELL (SNL-044, SNL-512, SNL-570; Wuhan, China), human normal oral keratinocytes (HOK) and OSCC cell lines (SCC-9 and CAL-27) were purchased from Procell (CP-H382, CL-0571, CL-0265; Wuhan, China).

THP-1 cells were cultured in RPMI-1640 medium (containing 10% fetal bovine serum (FBS) and 1% penicillin-streptomycin (P/S)) (SNM-

001E, SUNNCELL). SCC-9, SCC-25 and SCC-4 cells were cultured in DMEM/F12 medium (containing 10% FBS and 1% P/S) (SNM-004E, SUNNCELL). HOK and CAL-27 cells were cultured in DMEM medium (containing 10% FBS and 1% P/S) (SNM-002E, SUNNCELL). All cells were incubated at 37°C in a humidified atmosphere containing 5% CO_2 (3111, Thermo Fisher, Waltham, Massachusetts, USA), and the medium was replaced every 24 h. Cells were passaged at 70%-80% confluence. Cell line authentication was verified by short tandem repeat (STR) analysis. Mycoplasma contamination was routinely tested using a mycoplasma detection kit (CA1080, Solarbio, Beijing, China), and the results were confirmed to be negative.

HOK and OSCC cells were seeded at a density of 2×10^4 cells/well and treated with COP at concentrations of 0, 6.25, 12.5, 25, 50, 100 and 200 μM (HY-N0430, MedChemExpress, Shanghai, China) for 24 and 48 h, respectively. Subsequently, 10 μL Cell Counting Kit-8 (CCK-8) reagent (SNK-010, SUNNCELL) was added. Followed by incubation at 37°C for 2 h. The optical density (OD) at 450 nm was measured using microplate reader (SpectraMax iD3s, Molecular Devices, Shanghai, China) to determine the optimal treatment conditions.

SCC-9 cells were treated with 100 μM COP in the presence or absence of 1 μM mitochondrial-targeted antioxidant MitoQ (HY-100116A, MedChemExpress), 20 μM JAK2 inhibitor AG-490 (HY-12000, MedChemExpress), or 10 μM STAT3 activator Colivelin (HY-P1061, MedChemExpress) for 24 h [26-28].

Induced differentiation and co-culture of THP-1 cells

THP-1 cells were routinely cultured in medium containing 200 nM PMA (HY-18739, MedChemExpress) for 24 h to induce differentiation into M0 macrophages. For M1 polarization, M0 macrophages were further stimulated with 20 ng/mL interferon-γ (IFN-γ, P00028, Solarbio) and 100 ng/mL lipopolysaccharide (LPS, IL2020, Solarbio) for 24 h. For M2 polarization, M0 macrophages were treated with 20 ng/mL IL-4 (P0-0021, Solarbio) and 20 ng/mL IL-13 (P00131, Solarbio) for 24 h. THP-1 cells, M0, M1 and M2 macrophages were collected and cell morphology was observed under a microscope (Cytation5, BioTek, Winooski, Vermont, USA) [29].

THP-1 cells, as well as M1 and M2 macrophages, were treated with COP (1, 5, 10, 20, 40, 80, and 100 μM), 5 μg/mL anti-TNF-α (PHC3015L, Thermo Fisher), 20 μM AG490, or 10 μM Colivelin for 24 h. According to the Transwell non-contact co-culture model [30], THP-1 cells or polarized macrophages (M1 and M2), treated with COP (10, 20, and 40 μM), 5 μg/mL anti-TNF-α, 20 μM AG490, or 10 μM Colivelin, were seeded into the upper chamber of Transwell inserts (pore size 0.4 μm, 3401, Corning, NY, USA) at a density of 2×10^5 cells/mL. SCC-9 cells were seeded in the lower chamber at a density of 4×10^5 cells/well. After co-culture for 24 h, cells and culture supernatants from both chambers were collected for subsequent experiments.

Edu staining

OSCC cells were treated with 25, 50, and 100 μM COP for 24 h. The Edu working solution (SNK-014, SUNNCELL) was prepared according to the manufacturer's instructions, and pre-heated (37°C) EdU solution (20 μM) was added to each well of a 24-well plate in an equal volume, followed by incubation at 37°C for 2 h. Subsequently, cells were washed 1-2 times with PBS to remove unincorporated Edu. Cells were then fixed with 4% paraformaldehyde (P1110, Solarbio) for 30 min, permeabilized with 0.5% Triton X-100 (IR9073, Solarbio) for 15 min, and subsequently incubated with Click reaction solution for 30 min. Nuclear staining was performed using DAPI (ID22502, Solarbio) for 10 min. Positive fluorescence expression was observed and recorded under a microscope (IX73, Olympus, Tokyo, Japan).

Cell scratch test

SCC-9 and CAL-27 cells (2×10^6 cells/well) were seeded in 6-well plates. When the cell density reached approximately 90-100% confluence, a linear scratch was created using a sterile 100 μL pipette tip. Cells were then incubated with COP for 24 h. The scratch area was photographed by microscope at 0 h and 24 h, and the cell migration of each group was observed. Cell migration was evaluated by measuring the wound width using ImageJ software (NIH, Bethesda, MD, USA). Relative migration rate = (scratch width at 0 h - scratch width at 24 h)/scratch width at 0 h.

Transwell invasion assay

Matrix gel (356234, Solarbio) was thawed at 4°C and diluted with serum-free medium at a ratio of 1:8. Subsequently, 100 μL of diluted matrix gel was added to the upper chamber of Transwell inserts (24-well plate, 3422, Corning, NY, USA) and allowed to polymerize at 37°C for 0.5-1 h.

OSCC cells (4×10^4 cells/well) suspended in 100 μL serum-free medium were seeded into the upper chamber, while 500 μL medium containing 20% FBS was added to the lower chamber as a chemoattractant. After incubation at 37°C for 24 h, non-invading cells on the upper surface were gently removed using cotton swabs, whereas cells migrated to the lower surface were considered invasive cells. The invaded cells were fixed with 4% paraformaldehyde for 15 min and stained with 0.1% crystal violet (C0121, Beyotime, Shanghai, China) for 30 min. After washing, stained cells were observed and counted under a microscope.

Flow cytometry experiment

After intervention, OSCC cells were digested with trypsin, collected into flow cytometry tubes, and resuspended in 100 μL binding buffer. Subsequently, 5 μL PI and 5 μL Annexin V-FITC (E-CK-A211, Elabscience, Wuhan, China) were added. The samples were gently vortexed and incubated in the dark for 15 min at room temperature. After incubation, 400 μL binding buffer was added, and apoptotic cells were immediately analyzed using a flow cytometer (LSRFortessa, BD Biosciences, San Jose, California, USA).

The induced M1 and M2 macrophages were resuspended into single cell suspension (1×10^6 cells/100 μL). M1 macrophages were stained with anti-human CD86-FITC (374203, Biolegend, San Diego, CA, USA) and anti-human CD11b-APC (340007, Biolegend), while M2 macrophages were stained with anti-human CD206-PE (321105, Biolegend) and anti-human CD11b-APC (340007, Biolegend). After incubation at 4°C for 30 min in the dark, cells were resuspended in 500 μL paraformaldehyde fixative. M1 macrophages was determined as $CD86^+CD11b^+$ cells, whereas M2 macrophages were identified as $CD206^+CD11b^+$ cells. Polarization efficiency was subsequently quantified based on the percentage of positive cells.

Colony formation assay

OSCC cells were seeded into 35 mm culture dishes (430165, Corning, NY, USA) containing 2 mL complete medium. To ensure uniform cell distribution, the culture dishes were slowly rotated for 1 min after seeding. After cell attachment, the medium was replaced with fresh medium containing different concentrations of COP. Cells were cultured for approximately 14 days, during which cell growth and colony formation were monitored. Colonies with a diameter greater than 50 μm were considered valid colonies. At the end of the incubation, cells were fixed with 4% paraformaldehyde for 20 min and stained with 0.1% crystal violet (C0-121, Beyotime, Shanghai, China) for 10 min. After washing and air-drying, colonies were observed and counted under a microscope.

Western blot (WB)

Cells were harvested and lysed using RIPA buffer (P0013B, Beyotime) supplemented with a protease inhibitor mixture (P1005, Beyotime). After incubation on ice for 30 min, lysates were centrifuged at 12000 r/min for 15 min at 4°C, and the supernatants were collected as the total protein extracts. Protein concentrations was quantified using a BCA kit (P0010, Beyotime). Equal amounts of protein were denatured by boiling and separated by 12% sodium dodecyl sulfate-polyacrylamide gel electrophoresis (SDS-PAGE) (P0012A, Beyotime), followed by transfer onto polyvinylidene difluoride (PVDF) membranes (FFP39, Beyotime). After blocking with 5% skim milk (P0216, Beyotime) for 2 h, the membranes were incubated with primary antibodies overnight at 4°C. After washing, membranes were incubated with HRP-conjugated secondary antibody (ab205718, Abcam, Cambridge, UK) for 2 h at room temperature. Protein bands were visualized using an enhanced chemiluminescence (ECL) detection system (P0018M, Beyotime) and imaged with a ChemiDoc MP imaging system (Bio-Rad, CA, USA). Band intensities were quantified using ImageJ software, and target protein expression levels were normalized to GAPDH.

The primary antibody used in this study included E-cadherin (ab231303, 1:1000, Abcam), B-cell lymphoma 2 (Bcl2, ab32124, 1:1000, Abcam), N-cadherin (ab321897, 1:1000, Abcam), Vimentin (ab16700, 1:1000, Abcam),

Snail (ab216347, 1:1000, Abcam), Bcl2 associated X protein (Bax, ab53154, 1:1000, Abcam), caspase3 (ab32351, 1:5000, Abcam), JAK2 (ab39636, 1:1000, Abcam), p-JAK2 (ab195055, 1:2000, Abcam), cleaved-caspase3 (ab2302, 1:500, Abcam), IL-1β (ab216995, 1:1000, Abcam), iNOS (ab314088, 1:1000, Abcam), CD-206 (DF4149, 1:1000, Affinity, Jiangsu, China), IL-10 (ab133575, 1:1000, Abcam), Arginase 1 (Arg1, DF3791, 1:1000, Affinity), STAT3 (ab-68153, 1:2000, Abcam), p-STAT3 (ab76315, 1:1000, Abcam), and GAPDH (ab128915, 1:50000, Abcam).

Adenosine triphosphate (ATP) content

SCC-9 and CAL-27 cells were collected and lysed with 200 μL ATP lysis buffer (S0026, Beyotime) on ice, followed by centrifugation at 12 000 r/min for 5 min at 4°C. The supernatants were collected for analysis. In strict accordance with the instructions of ATP detection kit (S0026, Beyotime), 20 μL of supernatant was mixed with 100 μL of ATP working solution, and the OD value was measured immediately using a microplate reader. ATP concentrations were calculated based on a standard curve.

2',7'-dichlorofluorescein yellow diacetate (DCFH-DA) probe

DCFH-DA (D6471, Solarbio) was diluted in serum-free medium at a ratio of 1:1000 to obtain a final concentration of 10 μmol/L. Cells were incubated with 1 mL of the diluted DCFH-DA solution at 37°C for 20 min. After incubation, cells were resuspended with 500 μL PBS and immediately analyzed by flow cytometry to determine intracellular ROS levels.

Biochemical assay kits

Treated cells were collected and lysed on ice using an appropriate lysis buffer. After centrifugation at 4°C, the supernatants were collected. According to the manufacturer's protocol, commercial kits were used to measure superoxide dismutase (SOD, BC5165, Solarbio), malondialdehyde (MDA, BC6415, Solarbio) and glutathione/glutathione disulfide (GSH/GSSG, ab138-881, Abcam). Absorbance values were measured using a microplate reader, and the levels of SOD, MDA and GSH/GSSG were quantified according to standard curves.

Mitochondrial reactive oxygen species (mtROS) levels detected using MitoSOX Red

MitoSox Red (M4830, Solarbio) was diluted in PBS to prepare a 2 μmol/L staining working solution. After treatment, OSCC cells were incubated with 100 μL MitoSox Red staining solution at 37°C for 30 min. Subsequently, cells were washed with PBS to remove excess dye. Fluorescence was captured using a fluorescence microscope, and the average red fluorescence intensity (35 random fields) was quantified to evaluate mtROS levels.

Assessment of MMP levels using JC-1 probe

After removing the culture medium, OSCC cells were incubated with a mixture of fresh culture medium (1 mL) and JC-1 staining working solution (1 mL; M8650, Solarbio) at 37°C for 20 min. After incubation, cells were washed and resuspended in fresh medium.

Fluorescence images were acquired using an inverted microscope. Six random fields per group were selected for imaging. The fluorescence intensity of red and green signals were quantified using Image J software, and the ratio of red to green fluorescence was calculated to assess MMP levels.

Oxygen consumption rate (OCR) measurement

OSCC cells were seeded into Seahorse XF24 cell culture plates (103722-100, Agilent, Santa Clara, California, USA) at 1×10^6 cells/well and incubated overnight. Bioenergy detection was performed directly after cell intervention. Oligomycin (Oligo, 1 μM, 445851, Merck Millipore, Burlington, Massachusetts, USA) was injected to inhibit mitochondrial ATP production. Subsequently, carbonyl cyanide 4-(trifluoromethoxy) phenylhydrazone (FCCP; 2 μM; C2920, Sigma-Aldrich, St. Louis, Missouri, USA) was added to uncouple oxidative phosphorylation and determine maximal respiration. Finally, 0.5 μM rotenone (R8875, Sigma-Aldrich) and antimycin A (A8674, Sigma-Aldrich) were injected to inhibit complexes I and III, respectively, thereby determining non-mitochondrial respiration. OCR was measured at specified time intervals according to the manufacturer's protocol, and data were exported for subsequent analysis.

Enzyme-linked immunosorbent assay (ELISA)

Polarization markers were detected using ELISA kit. Kits for TNF-α, IL-12, IL-10, and transforming growth factor-β (TGF-β) were purchased from Elabscience (E-EL-H0109, E-EL-H0150, E-EL-H6154, E-EL-0162). Following treatment, cell culture supernatants were collected for analysis. 50 μL of standard solution was added to the standard wells. For sample wells, 10 μL of sample was mixed with 40 μL of sample diluent. Blank wells contained only assay buffer. Subsequently, 100 μL of enzyme-labeled antibody was added to each well (except blank wells), and the plate was incubated at room temperature for 60 min in the dark.

After incubation, the plate was rinsed 5 times and air-dried. Then, 50 μL of substrate A and B were added to each well and incubated for 15 min at 37°C in the dark. Finally, 50 μL stop solution was added to terminate the reaction. The OD value at 450 nm was immediately measured using a microplate reader. Cytokine concentrations were calculated based on standard curves.

Statistical analysis

Statistical analyses were performed using SPSS 27.0, and graphical presentations were realized using GraphPad Prism 9.0. All data were expressed as mean ± standard deviation (SD).

Normality of data distribution was assessed using the Shapiro-Wilk test, whereas homogeneity of variance was evaluated using the Lenvene's test, with $P > 0.05$ indicating normal distribution and equal variances. The Student's t-test was used for two-group comparison, and One-way ANOVA analysis followed by Tukey post hoc test were used for comparison among multiple groups. For data involving repeated measurements over time (e.g., OCR curves), Two-way repeated measures ANOVA was performed, with Bonferroni correction applied for multiple comparisons. A value of $P < 0.05$ was considered statistically significant.

Results

COP inhibited OSCC cell malignant phenotype

COP exhibited significant anti-cancer activity, and its chemical structure is shown in **Figure 1A**. In this study, treatment with 100 μM COP exerted minimal effects on the viability of normal human oral keratinocytes (HOK) (**Figure 1B**), suggesting that it had a good safety window for normal cells. However, COP significantly inhibited OSCC cell viability in a concentration- and time-dependent manner. Among them, SCC-9 and CAL-27 cells showed greater sensitivity to COP treatment (**Figure 1C-F**) and were therefore selected for subsequent study.

After treatment with 25, 50, and 100 μM COP for 24 h, Edu experiment demonstrated that the Edu fluorescence intensity significantly decreased (**Figure 1G-I**), indicating decreased DNA synthesis and proliferation. Moreover, COP treatment significantly delayed wound closure (**Figure 1J-L**) and reduced the number of invasive cells (**Figure 1M-O**), indicating that COP effectively suppressed OSCC cell migration and invasion ability. WB analysis of epithelial-mesenchymal transition (EMT)-related markers showed that COP treatment upregulated E-cadherin expressions and downregulated N-cadherin, Vimentin, and the key transcription factor Snail (**Figure 1P-T**). These findings indicate that COP significantly inhibits EMT, providing a mechanistic basis for its anti-metastatic effects.

COP induced apoptosis in OSCC cells

COP treatment significantly increased the apoptotic rate of OSCC cells (**Figure 2A-C**), confirming its pro-apoptotic effect. WB analysis also revealed that COP markedly upregulated the expression of pro-apoptotic proteins Bax and cleaved caspase-3, and significantly inhibited the anti-apoptotic protein Bcl-2 (**Figure 2D-G**). These results indicate that COP induces apoptosis in OSCC cells.

COP induced OSCC cell damage by promoting mitochondrial dysfunction and oxidative stress

Mitochondrial dysfunction and the resulting oxidative stress represent key mechanisms underlying tumor cell damage. Impaired mitochondrial function disrupts the electron transport chain, leading to excessive ROS production and eventually cell death. Due to the enhanced sensitivity of SCC-9 cells to COP, subsequent experiments were performed using SCC-9 cells.

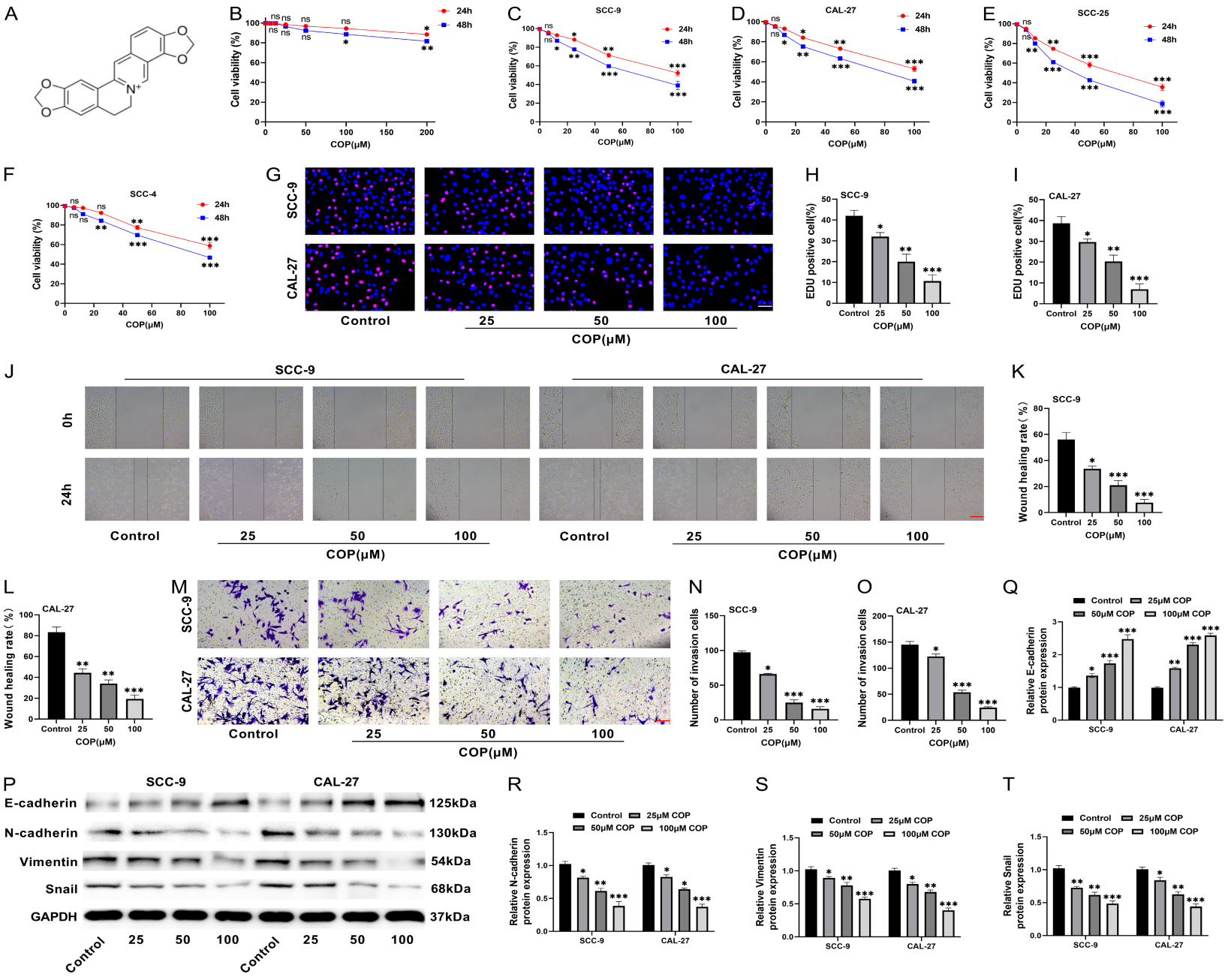
A
B
C
SCC-9
D
CAL-27
E
SCC-25
24h
48h
Cell viability (%)
COP(μM)
F
SCC-4
G
SCC-9
CAL-27
Control
25
50
100
H
EDU positive cell(%)
I
J
0h
24h
K
Wound healing rate (%)
L
M
N
Number of invasion cells
O
Q
Control
25μM COP
50μM COP
100μM COP
Relative E-cadherin protein expression
P
E-cadherin
N-cadherin
Vimentin
Snail
GAPDH
125kDa
130kDa
54kDa
68kDa
37kDa
R
Relative N-cadherin protein expression
S
Relative Vimentin protein expression
T
Relative Snail protein expression

Figure 1. Coptisine (COP) inhibited the malignant phenotype of oral squamous cell carcinoma (OSCC) cells. A: COP structure. B: Cell Counting Kit-8 (CCK-8) assay showing the effects of COP (0-200 μM) on the activity of normal oral keratinocytes (HOK). COP at 100 μM exhibited minimal effects on cell viability. C-F: CCK-8 assay showing the effects of COP (0-100 μM) on the viability of OSCC cell lines. COP significantly inhibited cell activity in a concentration-dependent manner. G-I: Edu incorporation assay showing that COP treatment significantly reduced OSCC cell proliferation (×40, 50 μm). J-L: Cell scratch assays demonstrating that COP treatment significantly suppressed cell migration (×10, 200 μm). M-O: Transwell invasion assays showing that COP treatment significantly reduced the invasion ability of OSCC cells (×20, 100 μm). P-T: Western blot analysis of epithelial-mesenchymal transition (EMT)-related protein expressions. COP significantly upregulated E-cadherin level and downregulated N-cadherin, Vimentin, and Snail expressions. $^{*}P < 0.05$, $^{**}P < 0.01$, $^{***}P < 0.001$ vs. Control group.

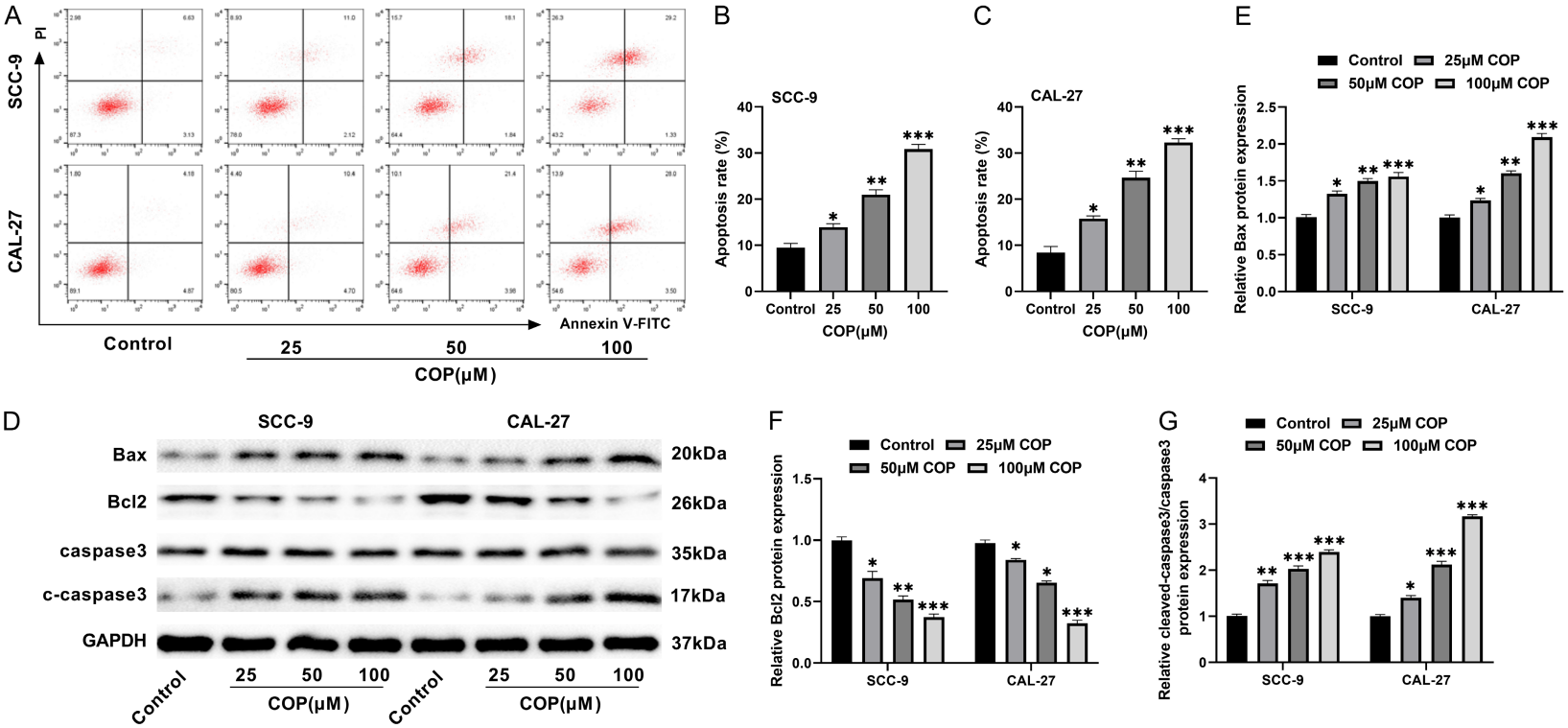

Figure 2. COP induced OSCC cell apoptosis. A-C: Flow cytometry analysis of apoptosis in OSCC cells. D-G: WB analysis of apoptosis-related proteins. $^{*}P < 0.05$, $^{**}P < 0.01$, $^{***}P < 0.001$ vs. Control group.

COP treatment markedly reduced intracellular ATP levels in SCC-9 cells (**Figure 3A**), indicating impaired energy production. Meanwhile, intracellular ROS levels were increased significantly after COP treatment (**Figure 3B**, **3C**). In addition, the levels of key antioxidant enzyme SOD and GSH/GSSG declined markedly, whereas the lipid peroxidation end product MDA was markedly increased (**Figure 3D-F**). Consistently, MitoSOX Red staining revealed a significant increase in mtROS levels (**Figure 3G**, **3H**), indicating the induction of oxidative stress.

Moreover, JC-1 staining showed an increase in green monomer fluorescence and a decrease in red aggregation fluorescence, indicating a significant reduction in mitochondrial membrane potential (MMP) (**Figure 3I**, **3J**) and impaired mitochondrial integrity and depolarization. Seahorse analysis further showed that COP significantly reduced OCR (**Figure 3K**), indicating impaired respiratory function. These findings demonstrate that COP induces pronounced mitochondrial dysfunction in OSCC cells.

Subsequently, SCC-9 cells were treated with COP (100 μM) in the presence or absence of mitochondrial-targeted antioxidant MitoQ (1 μM). MitoQ alone did no significantly affect colony formation, migration, or apoptosis in SCC-9 cells, indicating that MitoQ itself did not change the basal phenotype of SCC-9 cells under the experimental conditions. Compared with COP treatment alone, COP+MitoQ treatment significantly restored cell colony formation ability (**Figure 3L**, **3M**), increased cell migration and invasion ability (**Figure 3N-Q**), and significantly reduced COP-induced apoptosis (**Figure 3R**, **3S**). These results indicate that COP-induced mitochondrial dysfunction and oxidative stress are key upstream events mediating its inhibitory effects on the malignant phenotype of OSCC cells. In summary, COP exerts anti-tumor effects partially by inducing mitochondrial dysfunction and excessive mitochondrial oxidative stress.

COP promoted macrophage polarization toward the M1 phenotype and suppressed the malignant phenotype of OSCC cells

M1-polarized macrophages exert anti-tumor activity, whereas M2-polarized macrophages promote tumor growth and invasion. In this study, THP-1 cells were first induced with PMA to differentiate into M0 macrophages, followed by polarization into M1 and M2 phenotypes. Morphological observation revealed that the transparent spherical cells originally suspended in the culture medium gradually adhered and spread, with increased intercellular adhesion and stabilized morphology. M1 macrophages showed a rounded, flattened morphology, whereas M2 macrophages showed an elongated, fibroblast-like morphology (**Figure 4A**).

The proportion of $CD86^+CD11b^+$ M1 macrophages reached 88.0%, while $CD206^+CD11b^+$ M2 macrophages was 96.7% (**Figure 4B**, **4C**), indicating successful polarization. THP-1 cells were exposed to COP (0-100 μM) for 24 h, and concentrations ≤ 40 μM demonstrated little effects on cell viability (**Figure 4D**). Therefore, 10, 20, and 40 μM COP were selected for subsequent experiments.

Subsequently, COP was used to treat M1 and M2 macrophages. ELISA results showed that COP treatment significantly increased the secretion of M1-associated cytokines TNF-α and IL-12, characteristic pro-inflammatory factors, while reducing M2-associated cytokines IL-10 and TGF-β (**Figure 4E-H**). Consistently, COP markedly increased the proportion of $CD86^+$ macrophages and M1 markers (iNOS and CD86), while reducing the proportion of $CD206^+$ macrophages and M2 markers (Arg1, IL-10 and CD206) (**Figure 4I-P**). These findings indicate that COP specifically promotes macrophage polarization toward M1 type.

Using a Transwell co-culture system, the functional impact of COP-treated macrophages on OSCC cells was further evaluated. Co-culture with COP-treated, M1-polarized macrophages significantly reduced colony formation, migration, and invasion of SCC-9 cells (**Figure 4Q-V**), indicating significant inhibition of malignant phenotype of tumor cells.

To elucidate the contribution of M1 macrophage polarization to the anti-OSCC effects of COP, an anti-TNF-α antibody was used to block a key effector cytokine of M1 macrophages. Compared with the control group, COP-treated M1 macrophages significantly inhibited the proliferation, migration, and invasion of SCC-9 cells. It was worth noting that blockade of

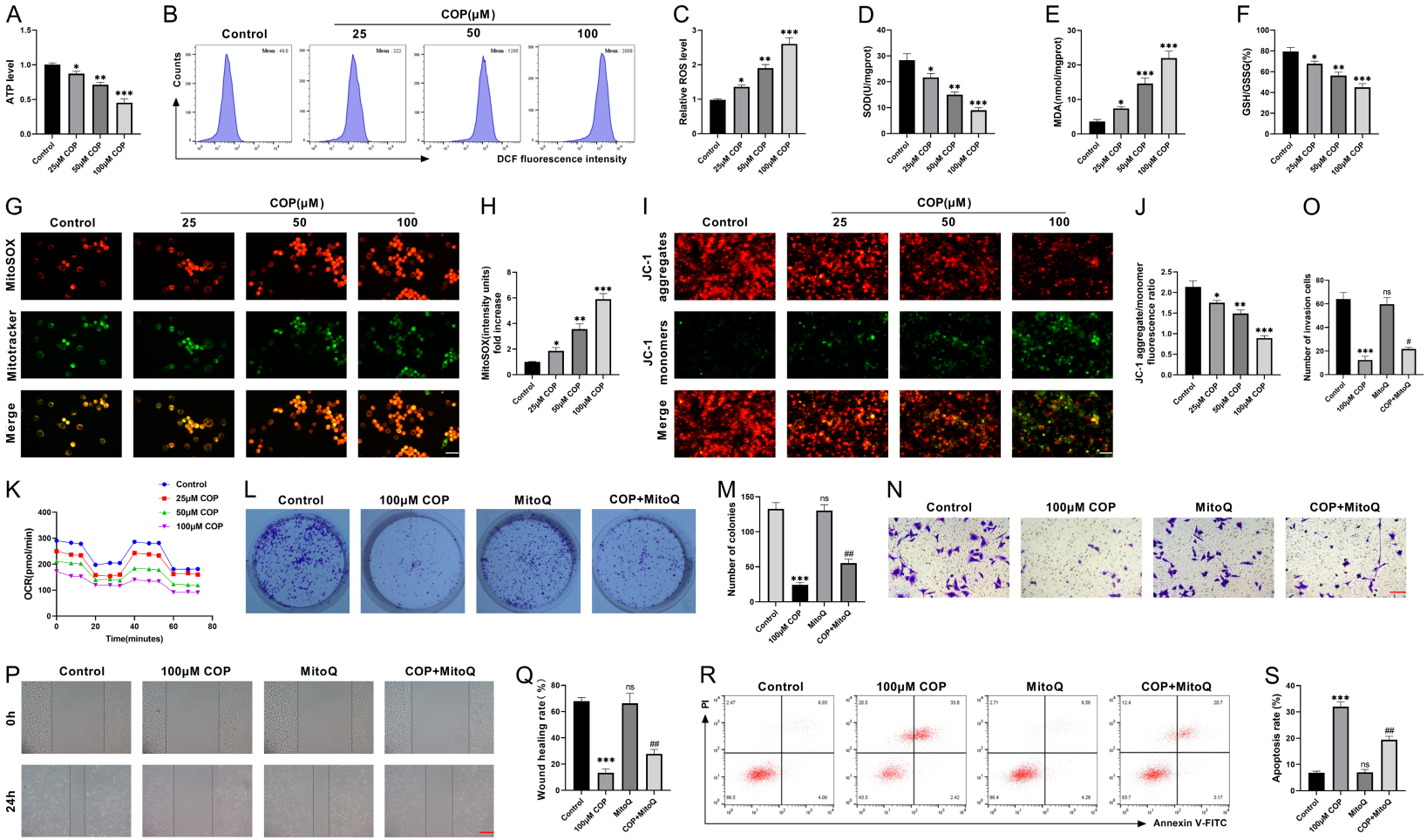

Figure 3. COP induced mitochondrial dysfunction and oxidative stress in OSCC cells. A: Intracellular adenosine triphosphate (ATP) levels were detected using a commercial kit. B, C: Intracellular reactive oxygen species (ROS) levels were detected using 2',7'-dichlorofluorescein yellow diacetate (DCFH-DA). D-F: Superoxide dismutase (SOD), malondialdehyde (MDA) and glutathione/glutathione disulfide (GSH/GSSG) were measured using assay kits. G, H: MitoSOX Red staining was used to evaluate the levels of mitochondrial reactive oxygen species (mtROS) in SCC-9 cells (×40, 50 μm). I, J: JC-1 staining was performed to assess mitochondrial membrane potential (MMP) (×40, 50 μm). K: Oxygen consumption rate (OCR) was measured using a Seahorse analyzer. L, M: Colony formation assays were performed to detect cell proliferation following co-treatment with COP and the mitochondrial-targeted antioxidant MitoQ. N, O: Transwell invasion assays showed that MitoQ treatment significantly increased after the invasive ability of SCC-9 cells (×20, 100 μm). P, Q: Cell scratch assays demonstrated that MitoQ treatment significantly enhanced cell migration (×10, 200 μm). R, S: Flow cytometry analysis showed that MitoQ treatment significantly reduced apoptosis in SCC-9 cells. Ns, not significant, $^{*}P < 0.05$, $^{**}P < 0.01$, $^{***}P < 0.001$ vs. Control group; $^{\#\#}P < 0.01$ vs. 100 μM COP group.

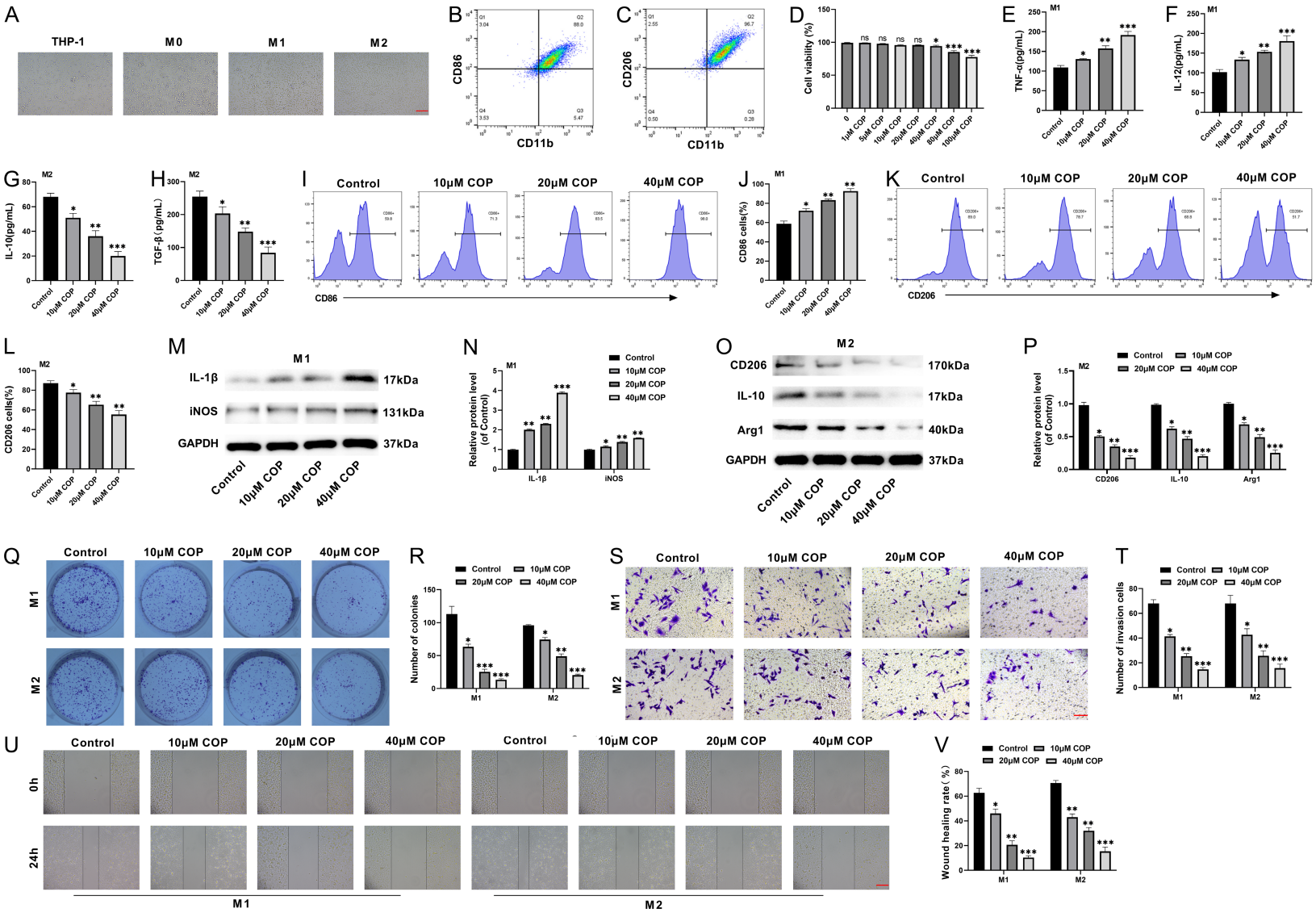
A
THP-1
M0
M1
M2
B
CD86
CD11b
C
CD206
CD11b
D
Cell viability (%)
0
1μM COP
5μM COP
10μM COP
20μM COP
40μM COP
80μM COP
100μM COP
E
M1
TNF-α(pg/mL)
Control
10μM COP
20μM COP
40μM COP
F
M1
IL-12(pg/mL)
G
M2
IL-10(pg/mL)
H
M2
TGF-β (pg/mL)
I
Control
10μM COP
20μM COP
40μM COP
CD86
J
M1
CD86 cells(%)
K
Control
10μM COP
20μM COP
40μM COP
CD206
L
M2
CD206 cells(%)
M
M1
IL-1β
17kDa
iNOS
131kDa
GAPDH
37kDa
Control
10μM COP
20μM COP
40μM COP
N
M1
Relative protein level (of Control)
Control
10μM COP
20μM COP
40μM COP
IL-1β
iNOS
O
M2
CD206
170kDa
IL-10
17kDa
Arg1
40kDa
GAPDH
37kDa
Control
10μM COP
20μM COP
40μM COP
P
M2
Relative protein level (of Control)
Control
10μM COP
20μM COP
40μM COP
CD206
IL-10
Arg1
Q
Control
10μM COP
20μM COP
40μM COP
M1
M2
R
Control
10μM COP
20μM COP
40μM COP
Number of colonies
M1
M2
S
Control
10μM COP
20μM COP
40μM COP
M1
M2
T
Control
10μM COP
20μM COP
40μM COP
Number of invasion cells
M1
M2
U
Control
10μM COP
20μM COP
40μM COP
Control
10μM COP
20μM COP
40μM COP
0h
24h
M1
M2
V
Control
10μM COP
20μM COP
40μM COP
Wound healing rate (%)
M1
M2

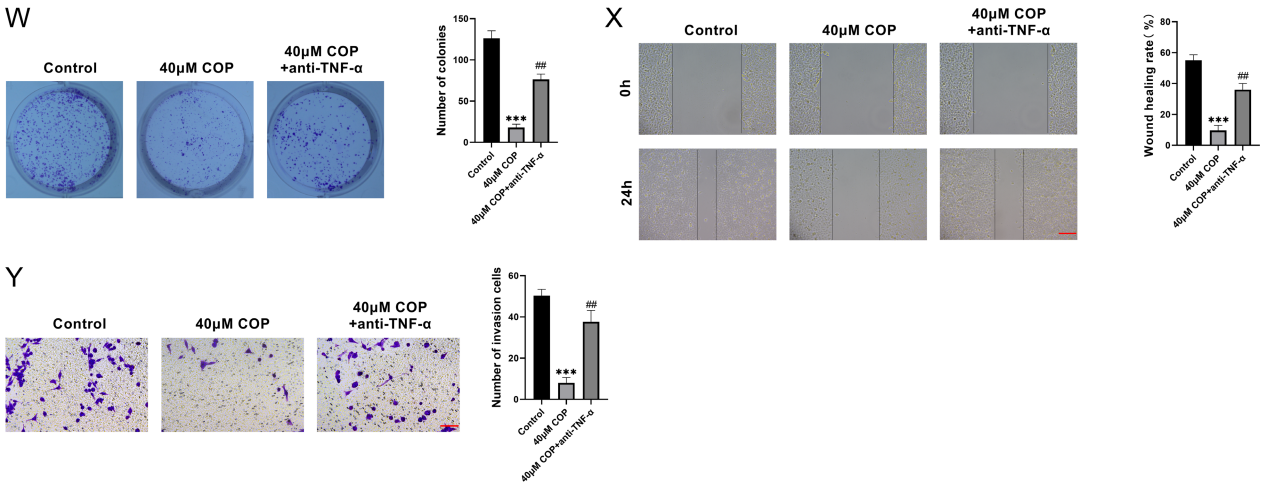

Figure 4. A-V: COP promoted macrophage polarization toward M1 phenotype and suppressed OSCC cell malignant phenotype. A: Morphological characteristics of THP-1 cells and differentiated M0, M1 and M2 macrophages were observed under a microscope (×20, 100 μm). B, C: Flow cytometry analysis of macrophage polarization: M1 macrophages identified as $CD86^+CD11b^+$ cells and M2 macrophages as $CD206^+CD11b^+$ cells. D: CCK-8 assay showing the effects of COP on THP-1 cell activity. E-H: Enzyme-linked immunosorbent assay (ELISA) of macrophage-associated cytokines following COP treatment. I-L: Flow cytometry analysis of $CD86^+$ and $CD206^+$ cell populations. COP treatment increased the proportion of $CD86^+$ cells and declined $CD206^+$ cells. M-P: WB analysis of macrophage polarization-specific proteins. COP significantly increased inducible nitric oxide synthase (iNOS) and CD86 protein levels and decreased Arginase 1 (Arg1), IL-10 and CD206 protein levels. Q, R: Colony formation assays of SCC-9 cells co-cultured with COP-treated M1 or M2 macrophages. S, T: Transwell invasion assays showing that COP treatment significantly reduced the invasive ability of SCC-9 cells (×20, 100 μm). U, V: Cell scratch assays demonstrating that COP treatment significantly inhibited cell migration (×10, 200 μm). ns, not significant, $^*P < 0.05$, $^{**}P < 0.01$, $^{***}P < 0.001$ vs. Control group. W-Y: Blocking M1 macrophage function attenuated the anti-tumor effect of COP on OSCC cells. W: Colony formation assay of SCC-9 cells co-cultured with COP-treated M1 macrophages in the presence or absence of anti-TNF-α. X: Wound healing assay showing that neutralization of TNF-α significantly enhanced the migration ability of SCC-9 cells. Y: Transwell invasion assay demonstrating that anti-TNF-α treatment significantly increased the invasive ability of SCC-9 cells (×20, 100 μm). $^{***}P < 0.001$ vs. Control group; $^{\#\#}P < 0.01$ vs. 40 μM COP group.

TNF-α significantly attenuated these inhibitory effects, manifested by increased colony formation, accelerated wound healing, and enhanced invasion (**Figure 4W-Y**).

These findings demonstrate that COP not only directly suppresses tumor cell growth but also modulates the TME by promoting macrophage polarization toward the M1 type, thus playing a dual anti-tumor role.

COP inhibited the JAK2/STAT3 signaling

The JAK2/STAT3 pathway is a canonical signaling cascade involved in inflammation and tumor progression. In SCC-9 cells, COP treatment significantly reduced the levels of p-JAK2 and p-STAT3 proteins, while exerting minimal effects on total JAK2 and STAT3 protein levels (**Figure 5A**, **5B**), indicating that COP specifically inhibits pathway activation. Treatment with AG490 (the JAK2 inhibitor) further enhanced the inhibitory effect of COP on this pathway, whereas Colivelin (the STAT3 activator) effectively reversed COP-mediated suppression of this pathway (**Figure 5C**, **5D**). Consistently, COP treatment also downregulated JAK2/STAT3 signaling in both M1 and M2 macrophages (**Figure 5E-G**), and AG490 further enhanced this inhibitory effect (**Figure 5H-J**). In summary, COP effectively suppresses JAK2/STAT3 signaling in both OSCC cells and macrophages.

COP induced mitochondrial dysfunction via the JAK2/STAT3 axis and suppressed OSCC cell growth

Compared with COP treatment alone, AG490 further reduced ATP production and MMP, while increasing intracellular ROS, mtROS, and MDA levels. In addition, AG490 further reduced SOD activity and the GSH/GSSG ratio, indicating aggravated mitochondrial dysfunction and oxidative stress. In contrast, Colivelin significantly reversed COP-induced mitochondrial impairment and oxidative stress (**Figure 6A-J**). Moreover, AG490 further inhibited the malignant phenotype of SCC-9 cells, whereas Colivelin had the opposite effect (**Figure 6K-P**). These findings indicate that COP induces mitochondrial dysfunction and inhibits malignant phenotypes of OSCC cells, at least partially through suppression of the JAK2/STAT3 signaling. Moreover, restoration of STAT3 activity by Colivelin partially rescued mitochondrial function and tumor cell phenotype; however, the addition of mitochondrial-targeted antioxidant MitoQ further restored the malignant phenotypes of OSCC cells, alleviated mitochondrial dysfunction and oxidative stress. These findings demonstrate that mitochondrial dysfunction and oxidative stress act as critical downstream mediators of JAK2/STAT3 signaling in COP-induced inhibition of OSCC cell growth.

COP promoted macrophage polarization toward M1 via the JAK2/STAT3 axis and suppressed OSCC cell growth

To investigate whether COP regulates polarization state of macrophages through the JAK2/STAT3 axis, M1 or M2 macrophages treated with COP alone or in combination with AG490 and Colivelin, and subsequently co-cultured with SCC-9 cells. Compared to COP intervention alone, co-treatment with AG490 enhanced M1 polarization, as evidenced by an increased proportion of $CD86^+$ cells and elevated TNF-α, IL-12, iNOS, and CD86 contents, and a simultaneous reduction in the proportion of $CD206^+$ cells and IL-10, TGF-β, Arg1, and CD206 levels. On the contrary, co-treatment with Colivelin effectively reversed the COP-induced M1 polarization and restored M2-related factor expression (**Figure 7A-L**).

Co-culture experiments showed that the malignant phenotype of SCC-9 cells was markedly inhibited after co-culture with COP-treated M1 macrophages, and this inhibitory effect was further enhanced by AG490 and partially reversed by Colivelin (**Figure 7M-R**). These findings indicate that COP promotes M1 macrophage polarization and inhibits OSCC malignant phenotypes at least in part via inhibiting the JAK2/STAT3 axis in macrophages.

To explore whether JAK2/STAT3 pathway inhibition by COP serves as a unified upstream mechanism connecting tumor cells and macrophages, a cross-co-culture experiment was performed. SCC-9 cells treated with COP, COP+AG490 and COP+Colivelin were collected and co-cultured with M1 or M2 macrophages, and then the polarization state of macrophages was detected. After co-culture with COP-treated SCC-9 cells, macrophages exhibited enhanced M1 polarization characteristics, including increased secretion of pro-inflammatory factors (TNF-α and IL-12), up-regulated expression

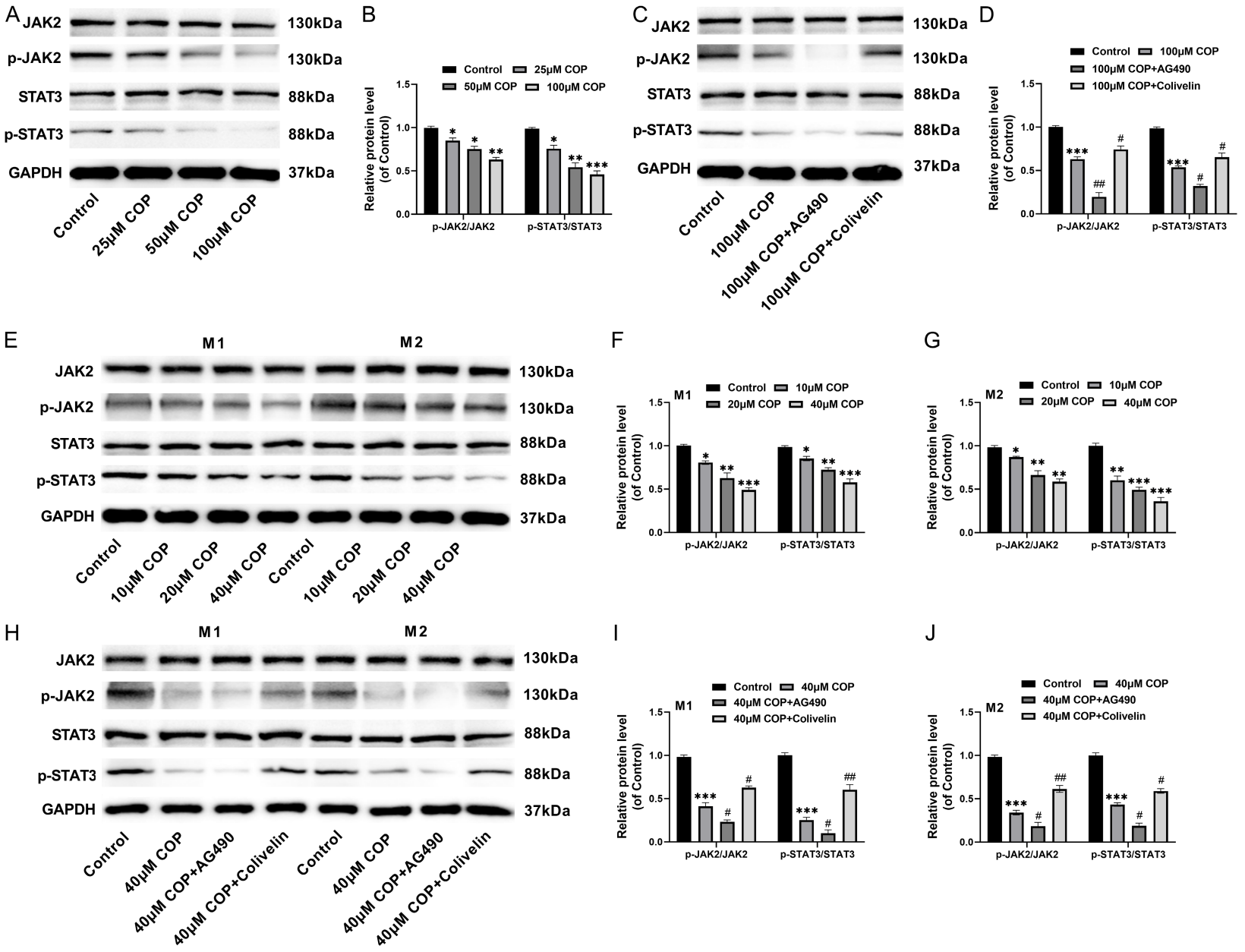
A
JAK2
p-JAK2
STAT3
p-STAT3
GAPDH
130kDa
130kDa
88kDa
88kDa
37kDa
Control
25μM COP
50μM COP
100μM COP
B
Control
25μM COP
50μM COP
100μM COP
Relative protein level (of Control)
p-JAK2/JAK2
p-STAT3/STAT3
C
JAK2
p-JAK2
STAT3
p-STAT3
GAPDH
130kDa
130kDa
88kDa
88kDa
37kDa
Control
100μM COP
100μM COP+AG490
100μM COP+Colivelin
D
Control
100μM COP
100μM COP+AG490
100μM COP+Colivelin
Relative protein level (of Control)
p-JAK2/JAK2
p-STAT3/STAT3
E
M1
M2
JAK2
p-JAK2
STAT3
p-STAT3
GAPDH
130kDa
130kDa
88kDa
88kDa
37kDa
Control
10μM COP
20μM COP
40μM COP
F
M1
Control
10μM COP
20μM COP
40μM COP
Relative protein level (of Control)
p-JAK2/JAK2
p-STAT3/STAT3
G
M2
Control
10μM COP
20μM COP
40μM COP
Relative protein level (of Control)
p-JAK2/JAK2
p-STAT3/STAT3
H
M1
M2
JAK2
p-JAK2
STAT3
p-STAT3
GAPDH
130kDa
130kDa
88kDa
88kDa
37kDa
Control
40μM COP
40μM COP+AG490
40μM COP+Colivelin
I
M1
Control
40μM COP
40μM COP+AG490
40μM COP+Colivelin
Relative protein level (of Control)
p-JAK2/JAK2
p-STAT3/STAT3
J
M2
Control
40μM COP
40μM COP+AG490
40μM COP+Colivelin
Relative protein level (of Control)
p-JAK2/JAK2
p-STAT3/STAT3

Figure 5. COP inhibited the Janus kinase 2/signal transducer and activator of transcription 3 (JAK2/STAT3) pathway. A, B: WB analysis of JAK2/STAT3 axis in SCC-9 cells. COP significantly decreased the protein levels of p-JAK2 and p-STAT3, with minimal effects on total protein levels. C, D: SCC-9 cells were treated with AG490 (JAK2 inhibitor) and Colivelin (STAT3 activator). WB analysis was performed to detect the JAK2/STAT3 signaling pathway. E-G: Western blot analysis of JAK2/STAT3 signaling in macrophages. H-J: M1 and M2 macrophages were treated with AG490 (JAK2 inhibitor) or Colivelin (STAT3 activator). WB detected JAK2/STAT3 axis proteins. $^{*}P < 0.05$, $^{**}P < 0.01$, $^{***}P < 0.001$ vs. Control group; $^{\#}P < 0.05$, $^{\#\#}P < 0.01$ vs. 100 μM COP/40 μM COP group.

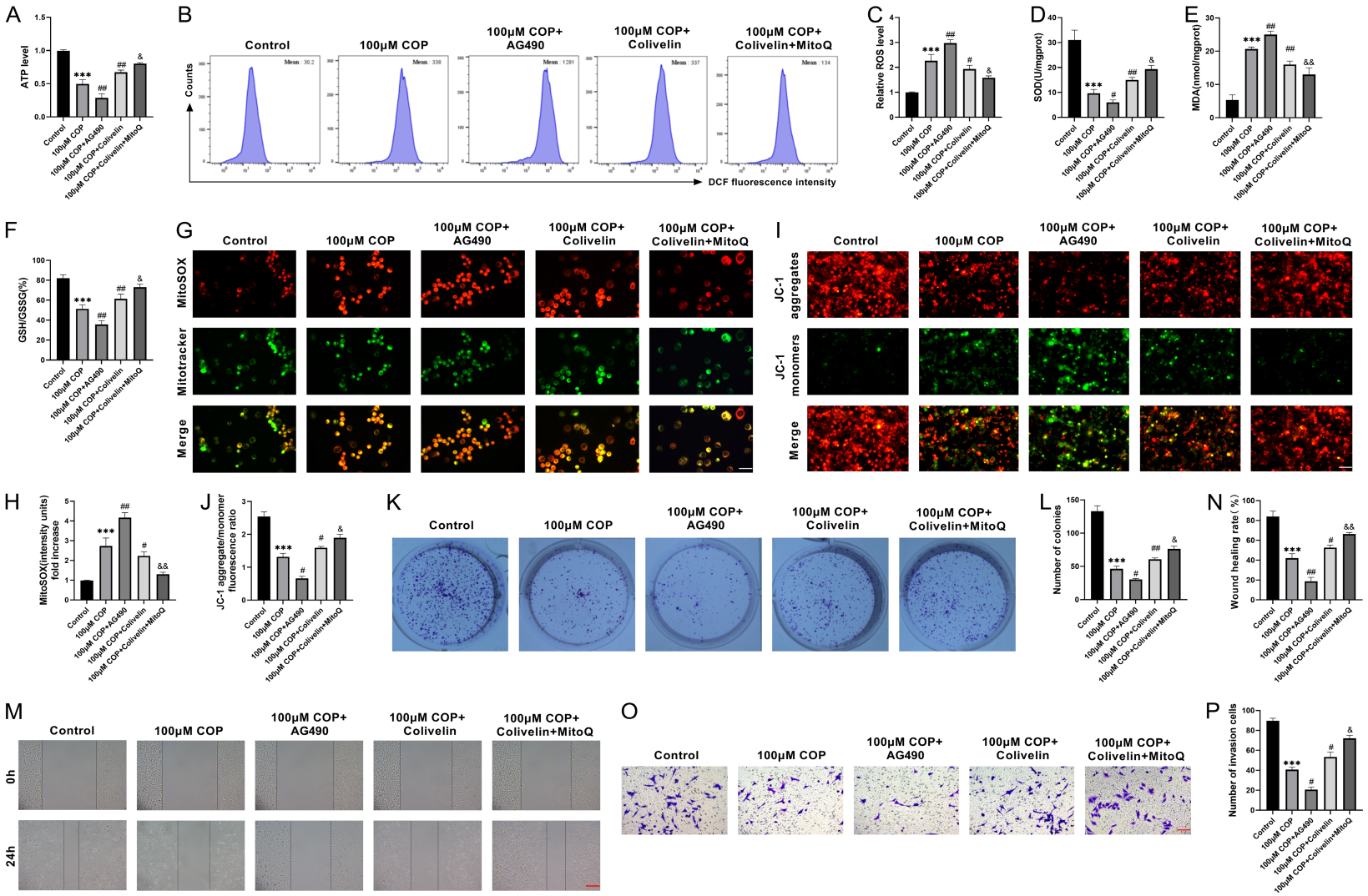

Figure 6. COP induced mitochondrial dysfunction in OSCC cells through JAK2/STAT3 axis and suppressed OSCC cell growth. A: Intracellular ATP level were measured using a commercial kit. Colivelin treatment significantly restored ATP levels compared with COP treatment. B, C: Intracellular ROS levels were detected using DCFH-DA. Colivelin treatment notably lessened reduced ROS levels. D-F: Oxidative stress-related indicators, including SOD, MDA and GSH/GSSG, were measured using assay kits. Colivelin treatment increased SOD activity and GSH/GSSG ration, while decreasing MDA contents. G, H: mtROS level in SCC-9 cells was measured using MitoSOX Red staining (×40, 50 μm). I, J: JC-1 staining was performed to assess MMP (×40, 50 μm). K, L: Colony formation assays showed that Colivelin treatment significantly restored the proliferative capacity of SCC-9 cells. M, N: Wound healing assays demonstrated that Colivelin treatment significantly enhanced cell migration (×10, 200 μm). O, P: Transwell invasion assays showed that Colivelin treatment significantly increased the invasive ability of SCC-9 cells (×20, 100 μm). $^{***}P < 0.001$ vs. Control group; $^{\#}P < 0.05$, $^{\#\#}P < 0.01$ vs. 100 μM COP group; $\&P < 0.05$, $\&\&P < 0.01$ vs. 100 μM COP+Colivelin group.

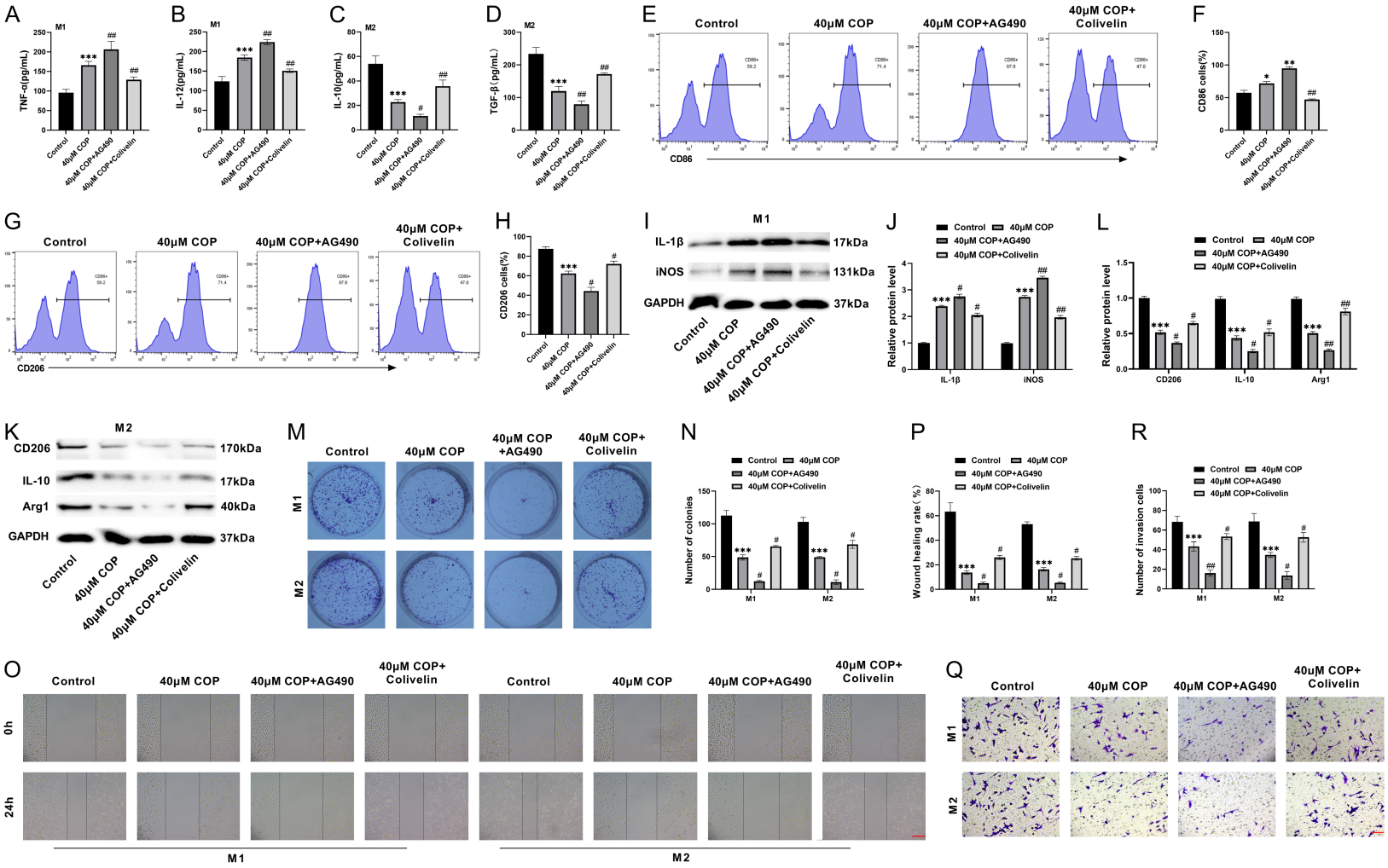

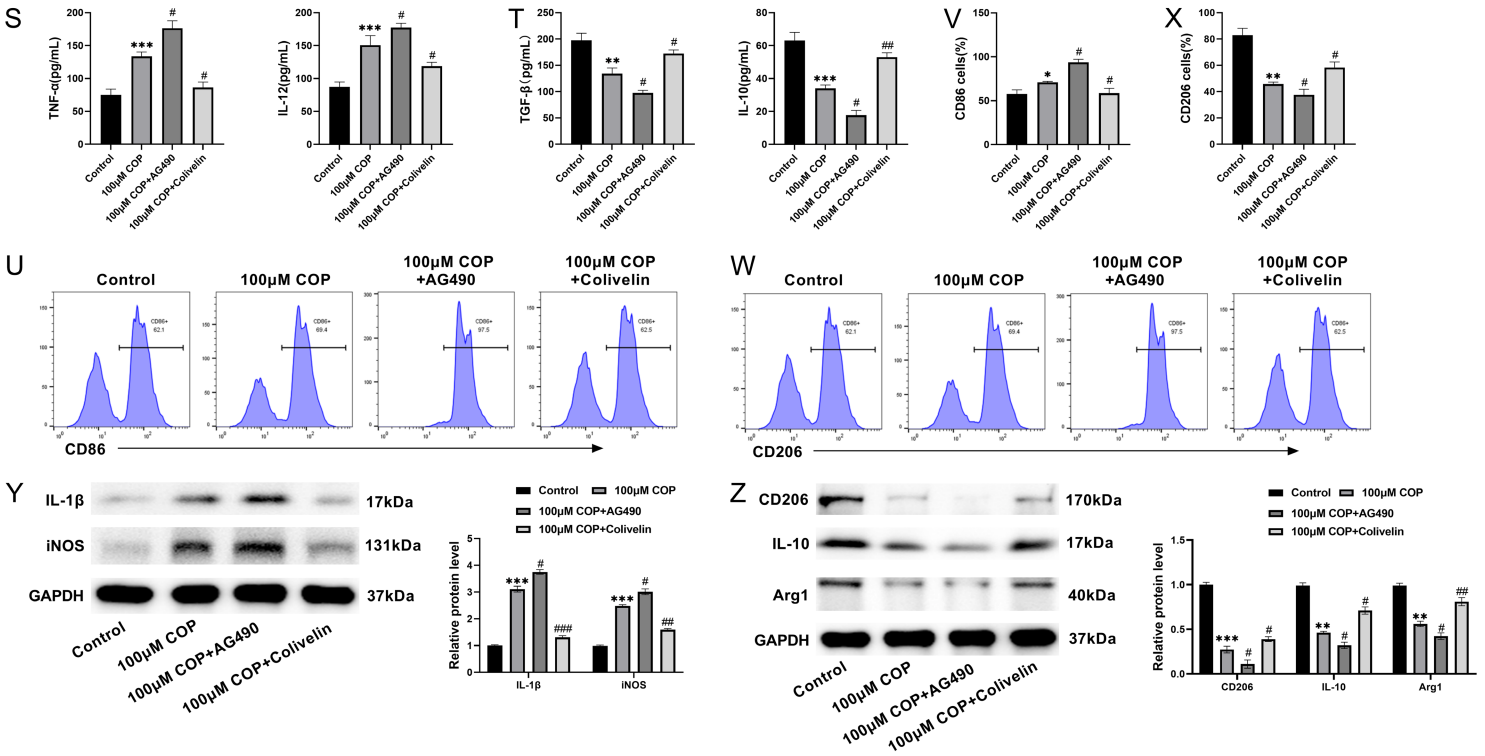

Figure 7. A-R: COP promoted macrophage polarization toward the M1 phenotype via the JAK2/STAT3 axis and suppressed OSCC cell growth. A-D: M1 or M2 macrophages treated with COP (40 μM) alone or in combination with AG490 (20 μM) or Colivelin (10 μM) were co-cultured with SCC-9 cells for 24 h. was performed to measure macrophage-related cytokines. Colivelin treatment significantly decreased TNF-α and IL-12 secretion, while increasing IL-10 and TGF-β levels. E-H: Flow cytometry analysis of $CD86^+$ and $CD206^+$ macrophage populations. Colivelin treatment decreased the proportion of $CD86^+$ cells and increased $CD206^+$ cells. I-L: WB analysis of macrophage polarization-specific proteins. Colivelin significantly downregulated iNOS and CD86 expression, while upregulating Arg1, IL-10 and CD206 expression. M, N: Colony formation assays of SCC-9 cells were co-cultured with macrophages treated with COP, AG490, or Colivelin. Colivelin treatment significantly restored the colony formation ability of SCC-9 cells. O, P: Wound healing assays showing that Colivelin treatment significantly enhanced the migration ability of SCC-9 cells (×10, 200 μm). Q, R: Transwell invasion assays demonstrating that Colivelin treatment significantly increased the invasive ability of SCC-9 cells (×20, 100 μm). $^*P < 0.05$, $^{**}P < 0.01$, $^{***}P < 0.001$ vs. Control group; $^{\#}P < 0.05$, $^{\#\#}P < 0.01$ vs. 100 μM COP group. S-Z: Inhibition of JAK2/STAT3 signaling pathway in SCC-9 cells promoted M1 polarization of co-cultured macrophages. S, T: SCC-9 cells treated with COP (100 μM) alone or in combination with AG490 (20 μM) or Colivelin (10 μM) were co-cultured with M1 or M2 macrophages for 24 h. The levels of M1 and M2 macrophage-related inflammatory factors were detected by ELISA. Colivelin significantly reduced the secretion of TNF-α and IL-12, and increased the levels of IL-10 and TGF-β. U-X: Flow cytometry was used to detect the proportion of $CD86^+$ and $CD206^+$ cells. Colivelin treatment significantly reduced the proportion of $CD86^+$ cells and increased the proportion of $CD206^+$ cells. Y, Z: WB analysis of macrophage polarization-specific proteins. Colivelin treatment significantly downregulated the protein levels of iNOS and CD86, and increased the protein levels of Arg1, IL-10 and CD206. $^*P < 0.05$, $^{**}P < 0.01$, $^{***}P < 0.001$ vs. Control group; $^{\#}P < 0.05$, $^{\#\#}P < 0.01$ vs. 100 μM COP group.

of M1 markers (CD86, iNOS, and IL-1β), and down-regulated expression of M2-related factors (IL-10, TGF-β, CD206, and Arg1) (**Figure 7S-Z**). Notably, co-treatment of SCC-9 cells with AG490 and COP further enhanced the induction of M1 polarization, whereas Colivelin-indued activation of STAT3 significantly attenuated this effect. These results suggest that inhibition of JAK2/STAT3 pathway in tumor cells constitutes a key upstream event that directs macrophage polarization toward the anti-tumor M1 phenotype. Collectively, our findings indicate that the JAK2/STAT3 pathway acts as not only a common molecular target of COP in tumor cells and macrophages, but also constitutes a continuous, cross-cell type signal axis.

Discussion

OSCC has an insidious onset and a high propensity for metastasis, imposing a serious clinical burden on OSCC patients. Therefore, identifying more effective therapeutic strategies has become a research hotspot. This study demonstrated that COP exerts a dual anti-tumor effect: it directly acts on OSCC cells, inducing mitochondrial dysfunction through inhibition of the JAK2/STAT3 pathway, eventually leading to cell death; in addition, COP can independently modulate macrophages, promoting their polarization toward the M1 phenotype via the same pathway. These findings suggest that COP has the dual potential of directly killing tumor cells and remodeling TME. However, the functional relationship between these two effects remains to be further elucidated.

Traditional Chinese medicine is an important part of clinical anti-cancer treatment due to its multi-target, multi-pathway mechanisms, which can improve immune function and inhibit tumor metastasis. COP has been reported to exhibit anti-inflammatory, antibacterial, and anti-tumor pharmacological effects. Qian *et al*. demonstrated that COP inhibits pyroptosis and proliferation while promoting apoptosis, thereby suppressing esophageal cancer growth [31]. Similarly, Yang *et al*. reported that COP exhibits anti-tumor activity in colon cancer, inhibiting tumor cell development and inducing apoptosis [32]. Yu *et al*. also showed that COP suppresses malignant biological behaviors in bladder cancer cells [33]. Similar to these studies, our results indicate that COP significantly inhibits OSCC cell proliferation, migration, and EMT, while promoting apoptosis, indicating that COP had good anti-OSCC potential.

Mitochondria, as the energy centers of cells, regulate various physiological processes, including cell energy production, metabolism, apoptosis, and ROS production. Evidence suggests that mitochondrial dysfunction contributes to cancer initiation and progression by affecting lipid metabolism, oxidative stress, and ROS production [34, 35]. Mitochondria, as a primary source of ROS, can stimulate the malignant progression of tumors when ROS production is dysregulated. Mitochondrial dysfunction is strongly associated with oral cancer development; for example, Lin *et al*. reported that plumbagin induced apoptosis of drug-resistant oral cancer cells through ROS-mediated mitochondrial dysfunction [36]. Previous studies have shown that COP can trigger autophagy in hepatocellular carcinoma by inducing ROS-mediated mitochondrial dysfunction [25]. Moreover, COP exerts anti-tumor effects by targeting mitochondrial complex I [22]. Consistently, our study demonstrated that COP treatment markedly promoted ROS and mtROS production in SCC-9 cells, decreased SOD activity, reduced GSH/GSSG ratio, diminished MMP, inhibited ATP production, and lowered OCR, suggesting that COP induces mitochondrial dysfunction in OSCC cells. Importantly, our study further highlighted the central role of mitochondrial damage: co-treatment with MitoQ, a mitochondrial-targeted antioxidant, significantly restored OSCC cell malignant phenotypes and inhibited apoptosis, confirming that mitochondrial dysfunction and oxidative stress are upstream events mediating the malignant phenotype of OSCC cells. STAT3, as a key link between membrane receptor signaling and mitochondrial function, has been shown to translocate to mitochondria to regulate the electron transport chain [37]. In this study, STAT3 activator Colivelin significantly reversed COP-induced mitochondrial dysfunction, whereas JAK2 inhibitor AG490 produced a synergistic effect, supporting the pivotal role of the JAK2/STAT3 pathway in maintaining mitochondrial homeostasis. These findings are consistent with observations in liver and breast cancers [20, 38], and further extend the functional scope of the JAK2/STAT3 pathway in tumor metabolic regulation.

TME is a main factor driving tumor invasion and metastasis [39]. TAMs are critical components

of TME and exhibit high heterogeneity, with different phenotypes exerting different functional effects [40]. Macrophages can be polarized into two major phenotypes: M1 macrophages, activated by stimuli such as LPS and TNF-α, secrete pro-inflammatory mediators and generate large amounts of ROS, thereby exerting anti-tumor effects; M2 macrophages, induced by IL-4 and IL-13, produce anti-inflammatory mediators, and can promote tumor progression [11, 41]. Tumor cells can induce macrophage polarization through secreted soluble proteins or cytokines, and polarized macrophages in turn regulate tumor invasion and metastasis [42-44]. M1 macrophages promote tumor invasion and metastasis [11]. In OSCC, TAMs signi ficantly influence tumor development, and the polarization state of TAMs is closely linked to disease progression. COP markedly promoted the polarization of macrophages toward the M1 phenotype, evidenced by increased secretion of pro-inflammatory factors, up-regulated M1 markers, and inhibited M2-related factors. Moreover, Co-culture experiments further revealed that SCC-9 cell proliferation, migration, and invasion were significantly inhibited when exposed to COP-treated M1 macrophages, demonstrating that COP promoted macrophage polarization toward the M1 subtype, thereby inhibiting the malignant phenotype of OSCC cells.

Mechanistically, the JAK2/STAT3 axis is abnormally activated in OSCC, driving tumor growth, metastasis, and immune evasion [45-47]. Upon ligand binding, JAK2 is phosphorylated and subsequently phosphorylates STAT3, which dimerizes and translocates to the nucleus to regulate transcription. This pathway also plays a central role in controlling mitochondrial function and macrophage polarization. Inhibition of this pathway can reduce mitochondrial damage and oxidative stress [48]. Shakya *et al*. reported that promoting mitochondrial superoxide production and down-regulating JAK2 and STAT3 phosphorylation can trigger tumor cell death [38], whereas pathway activation can promote tumor progression and macrophage M2 polarization [49]. Consistently, COP treatment markedly inhibited the JAK2/STAT3 axis. More importantly, STAT3 activator Colivelin reversed COP-induced mitochondrial damage and OSCC cell growth inhibition, while JAK2 inhibitor AG490 synergistically enhanced COP's effect. These results indicate that inhibition of the JAK2/STAT3 pathway is an upstream event of COP's direct anti-cancer effect. Moreover, COP promoted macrophage M1 polarization and inhibited OSCC growth via the same pathway in macrophages, highlighting a unified molecular mechanism linking tumor cell metabolism and immune modulation in the TME.

To further explore whether there is a functional correlation between the role of COP in tumor cells and macrophages, a cross-co-culture experiment was designed. The results showed that COP-treated SCC-9 cells could significantly induce macrophage polarization to the M1 phenotype. More importantly, when SCC-9 cells were treated with COP in combination with AG490, its induction of macrophage M1 polarization was further enhanced; whereas activation of STAT3 using Colivelin significantly attenuated this effect. These findings indicate that inhibition of the JAK2/STAT3 pathway in tumor cells serves as a key upstream event driving macrophage reprogramming. Biologically, the crosstalk between tumor cells and macrophages is a core issue of TME regulation [50, 51]. Tumor cells can domesticate infiltrating macrophages to obtain tumor-promoting phenotypes via secretion of cytokines, chemokines, exosomes, and other signaling molecules. In this study, COP was shown to reprogram macrophages into an anti-tumor M1 phenotype by inhibiting JAK2/STAT3 pathway in tumor cells, representing an indirect immune regulation mechanism.

However, several limitations should be acknowledged. First, the Transwell non-contact co-culture model used in this study, while useful for simulating indirect interactions between tumor cells and macrophages, cannot fully reflect the complexity of the *in vivo* TME. In tumor tissues, tumor-macrophage interactions are dynamic and influenced by many factors such as stromal cells, extracellular matrix, and hypoxia. Subsequent studies could employ a more complex three-dimensional co-culture systems to better simulate the *in vivo* TME. Second, reverse co-culture experiments using macrophage-conditioned medium could further clarify whether there is a bidirectional interactive regulation loop of 'macrophage-tumor cells'. Third, all experiments in this study were carried out *in vitro*, lacking validation in animal models. Future work should evaluate the *in vivo* anti-tumor

effects of COP in OSCC-bearing mouse models and elucidate the functional contribution of macrophages through macrophage depletion or adoptive transfer experiments. Additionally, conditional gene knockout models, such as specific STAT3 knockout mice, could provide further evidence for the core role of JAK2/STAT3 pathway in COP-mediated regulation of macrophage polarization *in vivo*.

Conclusion

This study systematically elucidated that COP exerts dual anti-tumor effects in OSCC. On the one hand, COP directly induces mitochondrial dysfunction in OSCC cells by inhibiting the JAK2/STAT3 pathway, leading to cell death. On the other hand, COP independently acts on macrophages, promoting their polarization to the M1 anti-tumor phenotype by inhibiting the same pathway, thereby suppressing tumor cell growth. These two paths have been verified based in independent experimental systems, the functional relationship between them requires further investigation. Collectively, these findings not only expand the pharmacological understanding of COP as an anti-cancer agent but also offer novel insights and an experimental basis for developing natural product-based OSCC therapies that integrate targeted and immune-modulatory strategies.

Disclosure of conflict of interest

None.

Abbreviations

COP, Coptisine; OSCC, oral squamous cell carcinoma; ROS, reactive oxygen species; MMP, mitochondrial membrane potential; TAMs, tumor associated macrophages; TME, tumor microenvironment; iNOS, inducible nitric oxide synthase; IL, interleukin; TNF-α, tumor necrosis factor-α; JAK2, Janus kinase 2; STAT3, signal transducer and activator of transcription 3; FBS, fetal bovine serum; P/S, penicillin-streptomycin; OD, optical density; PMA, phorbol 12-myristate 13-acetate; IFN-γ, interferon-γ; LPS, Lipopolysaccharide; Bcl2, B-cell lymphoma 2; Bax, Bcl2 associated X protein; Arg1, Arginase 1; ATP, Adenosine triphosphate; DCFH-DA, 2',7'-dichlorofluorescein yellow diacetate; SOD, superoxide dismutase; MDA, malondialdehyde; GSH/GSSG, glutathione/glutathione disulfide; mtROS, mitochondrial reactive oxygen species; OCR, oxygen consumption rate; TGF-β, transforming growth factor-β; EMT, epithelial-mesenchymal transition.

Address correspondence to: Feng Liu, Department of Acupuncture and Massage, Henan Vocational College of Tuina, No. 10, Xuefu Street, Luolong District, Luoyang 471023, Henan, China. E-mail: fengye6686liu@hotmail.com

References

[1] Yu Y, Niu J, Zhang X, Wang X, Song H, Liu Y, Jiao X and Chen F. Identification and validation of HOTAIRM1 as a novel biomarker for oral squamous cell carcinoma. Front Bioeng Biotechnol 2022; 9: 798584.

[2] Raza SH and Hameed Y. ERBB2 as a multifaceted biomarker in head and neck squamous cell carcinoma: in silico and in vitro evidence. Journal of Cancer Biomoleculars and Therapeutics 2025; 2: 1-14.

[3] Bray F, Laversanne M, Sung H, Ferlay J, Siegel RL, Soerjomataram I and Jemal A. Global cancer statistics 2022: GLOBOCAN estimates of incidence and mortality worldwide for 36 cancers in 185 countries. CA Cancer J Clin 2024; 74: 229-263.

[4] Xu Y, Jiang E, Shao Z and Shang Z. Long noncoding RNAs in the metastasis of oral squamous cell carcinoma. Front Oncol 2021; 10: 616717.

[5] Cui S, Liu H and Cui G. Nanoparticles as drug delivery systems in the treatment of oral squamous cell carcinoma: current status and recent progression. Front Pharmacol 2023; 14: 1176422.

[6] Abdel Hadi N, Reyes-Castellanos G and Carrier A. Targeting redox metabolism in pancreatic cancer. Int J Mol Sci 2021; 22: 1534.

[7] Jiang H, Fu Q, Yang J, Qin H, Li A, Liu S and Liu M. Blue light irradiation suppresses oral squamous cell carcinoma through induction of endoplasmic reticulum stress and mitochondrial dysfunction. J Photochem Photobiol B 2024; 257: 112963.

[8] Mottaghi M, Jafari F, Nejati M, Farshad F, Khorshidi Asl Z and Azmoudeh F. Mitochondrial DNA mutations in head and neck squamous cell carcinoma: a systematic review and meta-analysis. BMC Cancer 2025; 26: 76.

[9] Chen D, Zhang X, Li Z and Zhu B. Metabolic regulatory crosstalk between tumor microenvironment and tumor-associated macrophages. Theranostics 2021; 11: 1016-1030.

[10] Xiang X, Wang J, Lu D and Xu X. Targeting tumor-associated macrophages to synergize tu-

mor immunotherapy. Signal Transduct Target Ther 2021; 6: 75.
[11] You Y, Tian Z, Du Z, Wu K, Xu G, Dai M, Wang Y and Xiao M. M1-like tumor-associated macrophages cascade a mesenchymal/stem-like phenotype of oral squamous cell carcinoma via the IL6/Stat3/THBS1 feedback loop. J Exp Clin Cancer Res 2022; 41: 10.
[12] Christofides A, Strauss L, Yeo A, Cao C, Charest A and Boussiotis VA. The complex role of tumor-infiltrating macrophages. Nat Immunol 2022; 23: 1148-1156.
[13] Zhong Q, Fang Y, Lai Q, Wang S, He C, Li A, Liu S and Yan Q. CPEB3 inhibits epithelial-mesenchymal transition by disrupting the crosstalk between colorectal cancer cells and tumor-associated macrophages via IL-6R/STAT3 signaling. J Exp Clin Cancer Res 2020; 39: 132.
[14] Jiang M, Liu L, Huang W, Qi Y, Li Y and Li B. HMGB1-activated tumor-associated macrophages promote migration and invasion via NF-κB/IL-6 signaling in oral squamous cell carcinoma. Int Immunopharmacol 2024; 126: 111200.
[15] Mengie Ayele T, Tilahun Muche Z, Behaile Teklemariam A, Bogale Kassie A and Chekol Abebe E. Role of JAK2/STAT3 signaling pathway in the tumorigenesis, chemotherapy resistance, and treatment of solid tumors: a systemic review. J Inflamm Res 2022; 15: 1349-1364.
[16] Huma R, Mohammad A, Muhammad R, Muhammad Fawad A and Wadood A. STAT3 inhibition in cancer: a review of emerging therapeutics. Journal of Cancer Biomoleculars and Therapeutics 2025; 2: 65-73.
[17] Hu X, Xiang F, Feng Y, Gao F, Ge S, Wang C, Zhang X and Wang N. Neutrophils promote tumor progression in oral squamous cell carcinoma by regulating EMT and JAK2/STAT3 signaling through chemerin. Front Oncol 2022; 12: 812044.
[18] Xiao D, Zhu H and Xiao X. Knockdown of HM13 inhibits metastasis, proliferation, and M2 macrophage polarization of Non-small cell lung cancer cells by suppressing the JAK2/STAT3 signaling pathway. Appl Biochem Biotechnol 2025; 197: 570-586.
[19] Liu Y, Yi R, Zhang X, Sun X, Li J, Wang N, Yao X, Zhang C, Deng H, Wang S and Yang G. The mitochondrial dysfunction regulated by JAK2/STAT3 pathway leads to the necroptosis in the renal cells under patulin exposure. Ecotoxicol Environ Saf 2025; 296: 118202.
[20] Majid M, Tang B, Lai Y, Pang X, Ruan Y, Shi H, Peng W, Dai W and Hu X. Ficus pandurata as a functional phytotherapeutic: inhibiting JAK2/STAT3 signaling and activating mitochondrial apoptosis in hepatocellular carcinoma. Food Sci Nutr 2025; 13: e71114.
[21] Lu Q, Tang Y, Luo S, Gong Q and Li C. Coptisine, the characteristic constituent from coptis chinensis, exhibits significant therapeutic potential in treating cancers, metabolic and inflammatory diseases. Am J Chin Med 2023; 51: 2121-2156.
[22] Shen Y, Yang Y, Wang Z, Lin W, Feng N, Shi M, Liu J and Ma W. Coptisine exerts anti-tumour effects in triple-negative breast cancer by targeting mitochondrial complex I. Br J Pharmacol 2024; 181: 4262-4278.
[23] Nakonieczna S, Grabarska A, Gawel K, Wróblewska-Łuczka P, Czerwonka A, Stepulak A and Kukula-Koch W. Isoquinoline alkaloids from coptis chinensis franch: focus on coptisine as a potential therapeutic candidate against gastric cancer cells. Int J Mol Sci 2022; 23: 10330.
[24] Zhang YL, Zhang X, Miao XZ, Yuan YY, Gao J, Li X, Liu YG and Tan P. Coptisine suppresses proliferation and inhibits metastasis in human pancreatic cancer PANC-1 cells. J Asian Nat Prod Res 2020; 22: 452-463.
[25] Kim SY, Hwangbo H, Kim MY, Ji SY, Lee H, Kim GY, Kwon CY, Leem SH, Hong SH, Cheong J and Choi YH. Coptisine induces autophagic cell death through down-regulation of PI3K/Akt/mTOR signaling pathway and up-regulation of ROS-mediated mitochondrial dysfunction in hepatocellular carcinoma Hep3B cells. Arch Biochem Biophys 2021; 697: 108688.
[26] Hou D, Hu F, Mao Y, Yan L, Zhang Y, Zheng Z, Wu A, Forouzanfar T, Pathak JL and Wu G. Cationic antimicrobial peptide NRC-03 induces oral squamous cell carcinoma cell apoptosis via CypD-mPTP axis-mediated mitochondrial oxidative stress. Redox Biol 2022; 54: 102355.
[27] Jiang X, Huang Z, Sun X, Zheng X, Liu J, Shen J, Jia B, Luo H, Mai Z, Chen G and Zhao J. CCL18-NIR1 promotes oral cancer cell growth and metastasis by activating the JAK2/STAT3 signaling pathway. BMC Cancer 2020; 20: 632.
[28] Xie JR, Chen XJ and Zhou G. Nuciferine inhibits oral squamous cell carcinoma partially through suppressing the STAT3 signaling pathway. Int J Mol Sci 2023; 24: 14532.
[29] Wang P, Tao L, Yu Y, Wang Q, Ye P, Sun Y and Zhou J. Oral squamous cell carcinoma cell-derived GM-CSF regulates PD-L1 expression in tumor-associated macrophages through the JAK2/STAT3 signaling pathway. Am J Cancer Res 2023; 13: 589-601.
[30] Zhang Y, Liu S, Qu D, Wang K, Zhang L, Jing X, Li C, Wei F and Qu X. Kif4A mediate the accumulation and reeducation of THP-1 derived macrophages via regulation of CCL2-CCR2 expression in crosstalking with OSCC. Sci Rep 2017; 7: 2226.

[31] Qian C, Zhang X, Tian YS, Yuan L, Wei Q, Yang Y, Xu M, Wang X and Sun M. Coptisine inhibits esophageal carcinoma growth by modulating pyroptosis via inhibition of HGF/c-Met signaling. Naunyn Schmiedebergs Arch Pharmacol 2025; 398: 8375-8389.
[32] Yang J, Tao Q, Li J, Xie Y, Tang C, Huang X, Chen Y and Zeng C. Exploring the molecular targets and therapeutic potential of coptisine in colon cancer: a network pharmacology approach. Curr Med Chem 2025; 32: 3295-3308.
[33] Xiaohui Y, Jie L and Jiangqiao Z. Coptisine regulates PI3K/AKT pathway to block bladder cancer progression: a study based on network pharmacology, in vitro and in vivo assays. Hereditas 2025; 162: 232.
[34] Kenny TC and Birsoy K. Mitochondria and cancer. Cold Spring Harb Perspect Med 2024; 14: a041534.
[35] Wang SF, Tseng LM and Lee HC. Role of mitochondrial alterations in human cancer progression and cancer immunity. J Biomed Sci 2023; 30: 61.
[36] Lin CL, Yu CI, Lee TH, Chuang JM, Han KF, Lin CS, Huang WP, Chen JY, Chen CY, Lin MY and Lee CH. Plumbagin induces the apoptosis of drug-resistant oral cancer in vitro and in vivo through ROS-mediated endoplasmic reticulum stress and mitochondrial dysfunction. Phytomedicine 2023; 111: 154655.
[37] Zheng ZY, Yang PL, Li RY, Liu LX, Xu XE, Liao LD, Li X, Chu MY, Peng L, Huang QF, Heng JH, Wang SH, Wu ZY, Chang ZJ, Li EM and Xu LY. STAT3β disrupted mitochondrial electron transport chain enhances chemosensitivity by inducing pyroptosis in esophageal squamous cell carcinoma. Cancer Lett 2021; 522: 171-183.
[38] Shakya R, Park GH, Joo SH, Shim JH and Choi JS. Hydroxyzine induces cell death in triple-negative breast cancer cells via mitochondrial superoxide and modulation of Jak2/STAT3 signaling. Biomol Ther (Seoul) 2022; 30: 585-592.
[39] Li Y, Ma Z, Li W, Xu X, Shen P, Zhang SE, Cheng B and Xia J. PDPN+ CAFs facilitate the motility of OSCC cells by inhibiting ferroptosis via transferring exosomal lncRNA FTX. Cell Death Dis 2023; 14: 759.
[40] Zhang H, Liu L, Liu J, Dang P, Hu S, Yuan W, Sun Z, Liu Y and Wang C. Roles of tumor-associated macrophages in anti-PD-1/PD-L1 immunotherapy for solid cancers. Mol Cancer 2023; 22: 58.
[41] Yan S and Wan G. Tumor-associated macrophages in immunotherapy. FEBS J 2021; 288: 6174-6186.
[42] Lin Y, Zhang W, Liu L, Li W, Li Y and Li B. ENO1 promotes OSCC migration and invasion by orchestrating IL-6 secretion from macrophages via a positive feedback loop. Int J Mol Sci 2023; 24: 737.
[43] Lin Y, Qi Y, Jiang M, Huang W and Li B. Lactic acid-induced M2-like macrophages facilitate tumor cell migration and invasion via the GPNMB/CD44 axis in oral squamous cell carcinoma. Int Immunopharmacol 2023; 124: 110972.
[44] Wang L, Wang C, Tao Z, Zhu W, Su Y and Choi WS. Tumor-associated macrophages facilitate oral squamous cell carcinomas migration and invasion by MIF/NLRP3/IL-1β circuit: a crosstalk interrupted by melatonin. Biochim Biophys Acta Mol Basis Dis 2023; 1869: 166695.
[45] Lu Y, Yao M, Wang D, Higuchi D, Lu H, Shang H, Dong B, Zhang J, Jin R and Liu T. CMSP suppresses oral squamous cell carcinoma progression by targeting the JAK2/STAT3/c-Myc axis. Front Oncol 2025; 15: 1671797.
[46] Cao M, Tian K, Sun W, Xu J, Tang Y and Wu S. MicroRNA-141-3p inhibits the progression of oral squamous cell carcinoma via targeting PBX1 through the JAK2/STAT3 pathway. Exp Ther Med 2022; 23: 97.
[47] Zhang Z, Guo T and Zhao X. SIRT7-mediated MVP desuccinylation facilitates tongue squamous cell carcinoma progression by activating JAK2/STAT3 pathway. Cell Biol Int 2025; 49: 1184-1196.
[48] Zhang H, Gui Y, Che W, Deng S and Yang L. SOCS2 alleviates traumatic brain injury-induced mitochondrial damage and parthanatos in endothelial cells by inhibiting the JAK2/STAT3 signaling pathway. Metab Brain Dis 2025; 40: 289.
[49] Li S, Dong Q, Ren W, Sun Y, Wang Z and Pan L. TFAP4/DLGAP5 promotes tumor progression and macrophage M2 polarization in prostate cancer by activating the JAK2/STAT3 signaling. Exp Cell Res 2025; 452: 114753.
[50] Zhou X, Liu Q, Wang X, Yao X, Zhang B, Wu J and Sun C. Exosomal ncRNAs facilitate interactive 'dialogue between tumor cells and tumor-associated macrophages. Cancer Lett 2023; 552: 215975.
[51] Yao M, Mao X, Zhang Z, Cui F, Shao S and Mao B. Communication molecules (ncRNAs) mediate tumor-associated macrophage polarization and tumor progression. Front Cell Dev Biol 2024; 12: 1289538.